RSC Advances

ROYAL SOCIETY OF CHEMISTRY

www.rsc.org/advances

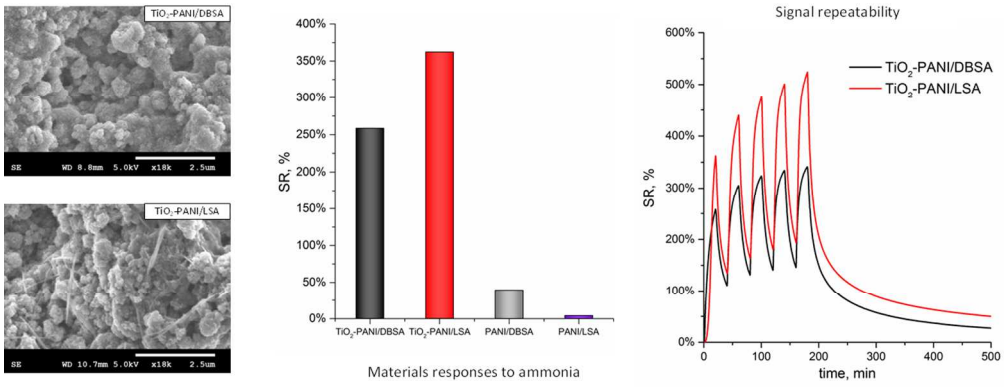

Morphology and sensor responses
352x138mm (96 x 96 DPI)

Cite this: DOI: 10.1039/x0xx00000x

Ammonia/amines electronic gas sensors based on hybrid polyaniline-TiO_2 nanocomposites. The effects of titania and the surface active doping acid

S. Mikhaylov[a,b], N. Ogurtsov[a], Yu. Noskov[a], N. Redon[b], P. Coddeville[b], J-L. Wojkiewicz[b*] and A. Pud[a*]

Received ooth January 2012,
Accepted ooth January 2012

DOI: 10.1039/x0xx00000x

www.rsc.org/

New ammonia and amines sensing materials based on hybrid polyaniline/titanium dioxide nanocomposites were synthesized by a one-pot chemical polymerization. Particular attention was paid to the influence of TiO_2 nanoparticles and the surface active dopants on structure-property relationship of the nanocomposites in terms of their morphology, composition, electrical and sensing properties. Dodecylbenzenesulfonic (DBSA) and lauryl sulfuric (LSA) acids were used as polyaniline dopants. The nanocomposites sensing properties were evaluated at different humidity levels when exposed to ammonia, methyl- and trimethylamine (0.2 ppm – 1ppm). The materials demonstrated strong responses and high sensitivity to the gases with the quantification limit of 20 ppb for ammonia. The sensors are reversible and have short response times. However, the response magnitude depends on dopant nature. The results were interpreted in terms of basicity and size of the analyte gas molecules.

Keywords: polyaniline, titanium dioxide, nanocomposites, gas sensor, ammonia, amines.

Introduction

The anthropogenic atmospheric pollution is associated with the road transport emissions, industry and power plants, refineries and agricultural activities [1, 2]. In particular, concentrations of such toxic gases as ammonia and amines continuously increased since the XIX century. Their tendency to interact with $^{\cdot}OH$ and $^{\cdot}NO_3$ radicals, ozone and Cl atoms in the atmosphere in complex ways leads to the formation of potentially harmful and toxic products (e.g. hydrogen cyanide, formic acid, formaldehyde) affecting both human health and environment [3-6].

Therefore, ammonia and amines concentrations monitoring is an important step towards air quality improvement. The known analytical techniques like gas/liquid chromatography coupled with different detectors [7, 8], ion mobility spectrometry [9, 10], photoacoustic spectroscopy [11-14], surface-enhanced Raman scattering [15-18], capillary electrophoresis [19-21] usually utilize expensive, bulky and quite sophisticated equipment. That is why such compact portable solutions allowing rapid local real-time detection as electronic sensors are a promising alternative to time-consuming laboratory techniques. The principle of operation is a quite simple conversion of chemical changes in sensing layer into electrically measurable response signal. In this regard the application of intrinsically conducting polymers (ICP) able to reversibly change their characteristics depending on atmosphere composition is a promising direction in a development of sensing materials [22-25]. In this regard, one of the most prominent ICPs is polyaniline (PANI) due to its ability to participate in typical acid-base interactions [26-28]. In particular, contact of acids doped PANI with basic substances leads to its dedoping by deprotonation and can be used for ammonia/amines concentrations determination (Fig. 1) [25].

The dopant choice significantly influences the polymer sensitivity to pollutants and predetermines its structure, morphology, hydrophobicity and conductivity [29, 30]. An improvement of response time, sensitivity, detection limit, stability and durability can be usually achieved by aniline polymerization in a presence of semiconducting metal oxides nanoparticles (e.g TiO_2, ZnO, SnO_2 etc) [31-34].

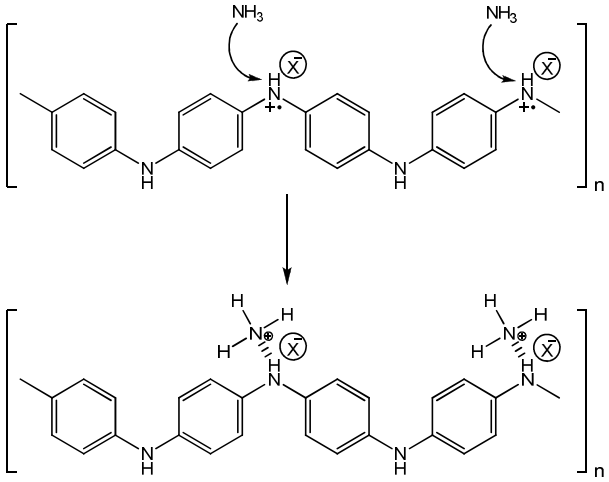

Fig. 1. Scheme of PANI-ammonia interactions forming sensor response [25].

This approach allows formation of high surface/volume ratio nanocomposites and facilitates penetration of the analyte gas molecules inside the sensing layer [35]. Furthermore, Gong et al [36] reported about formation of a diode-like nanostructure that functions as electric current switch when NH_3 gas is absorbed by PANI and permits detection at ppt levels.

However, the metrological parameters of sensors vary in different papers and strongly depend on preparation conditions and methods [37, 38]. Probably this variability is additionally caused by the interaction and interference of factors having different nature and thus affecting PANI synthesis kinetics and resulting properties in unexpected ways.

Trying to shed more light on these aspects we have synthesized, studied and compared properties of pure PANI and its TiO_2 based nanocomposites doped with two surface active acids i.e. dodecylbenzenesulfonic acid (DBSA) and lauryl sulfuric acid (LSA). This approach allowed us to determine effects of both titania and

these acids on the obtained materials structure and sensitivity to ammonia, methylamine (MA) and trimethylamine (TMA).

Experimental

Materials

Aniline (Merck) was distilled under vacuum and stored under argon at 3-5 °C. The reagent grade ammonium persulfate (APS) (Ukraine) and DBSA (Acros), TiO_2 anatase nanoparticles 5-10 nm (MTI Corporation) were used as received. The LSA was prepared from sodium lauryl sulfate (Aldrich) via ion exchange reaction with resin KU-2-8 (Ukraine).

The nanocomposites synthesis

The typical oxidative aniline polymerization procedure described elsewhere [35] was used with some modifications for the nanocomposites formation. In short, the fabrication process involved the aniline polymerization at 10 °C under action of ammonium persulfate in the presence of TiO_2 nanoparticles (Specific surface area = 210 m^2/g) dispersed in the solutions of the anilinium salts of DBSA or LSA. The initial weight ratio of aniline to TiO_2 in the polymerization mixture was 1:10. The used aniline:oxidant:acid molar ratios were 1:1.25:1.5. The formed core-shell PANI nanocomposites were purified by dialysis against distilled water for 72 hours and dried under vacuum at 60 °C to a constant weight.

Sensing layer preparation

The experimental procedure included few steps. At first, synthesized pure PANI and nanocomposites were dispersed in dichloroacetic acid (DCAA) and homogenized in ultrasonic bath. The samples were deposited onto Au/ceramic interdigitated electrodes (Synkera Inc.) by drop-casting and dried under vacuum at 80°C for 72 hours. The multisensors card comprising electrodes array with investigated materials was placed inside thermostabilized exposure chamber [39].

Samples testing procedure

The metrological sensing parameters of the synthesized materials were measured using a flow-type experimental system described elsewhere [35]. All the experiments were conducted at constant temperature (25±0.5°C) and different relative humidity (RH) levels. The tested concentration ranges were 0.2 – 1 ppm for methylamine (MA), trimethylamine (TMA) and ammonia. The sensor responses (SR) to these analytes were calculated as relative change of the sample resistance ($R-R_0$), comparing to initial resistance value (R_0): $SR = [(R-R_0)/ R_0]\times100\%$.

The sensors resistance changes were continuously measured with a digital multimeter (Agilent 34970A) as a function of pollutant concentrations and exposure time. The desired analyte concentration inside chamber was generated using mass flow controllers by mixing pollutant from a standard gas cylinder (PRAXAIR Company) with purified air from a zero air generator (Whattman 76-804).

The measurement protocol involved three stages. At first, the initial resistance R_0 was estimated as a mean value of sensing material resistance measured during 5 minutes in the flow of purified air. Then, after exposition to a pollutant sensors changed their resistance due to interaction of active layer (PANI composites) with the analyte molecules. Finally, the sensor was flushed with air from zero air generator, resulting in desorption of adsorbed pollutant molecules and resistance decrease to its initial values level [27]. To determine the RH influence on the sensor response, the sensors were submitted to 20, 35, 50, 65 and 80% of relative humidity. We have to note, that at high humidity levels the effect of water vapour on the ammonia response is difficult to determine precisely because the moisture reacts with ammonia producing ammonium hydroxide.

Characterization

The Fourier Transform Infrared Spectroscopy (FTIR) spectra of PANI composites were recorded on Bruker Vertex 70 spectrometer at resolution of 1 cm^{-1}. The XRD measurements were carried on the automatic computer-controlled X-ray diffractometer DRON-3M with CuKα radiation (λ = 1.541 Å). Small-angle X-ray scattering (SAXS) data are reported in reciprocal space as intensity *vs* the scattering vector magnitude (q), where $q = (4\pi\cdot\sin\theta)/\lambda$. Transmission and scanning electron microscopy (TEM and SEM) images were obtained with a help of the JEOL JEM-1400 and HITACHI S-4300 SE/N microscopes respectively. The specific surface area (SSA) was measured by Brunauer-Emmett-Teller (BET) method .

Results and discussion

The nanocomposites morphology

The effect of the surface active dopants on the synthesized nanocomposites morphology was visualized by TEM and SEM methods. The used titanium dioxide nanoparticles (Fig. 2a) have asymmetric rice-like form with the average length about 20-30 nm and diameter of about 10-15 nm. The TiO_2 particles do not change their shape and appear to be completely occluded with PANI matrix after the synthesis (Fig. 2b-c). The detailed analysis of enlarged TiO_2-PANI/DBSA and TiO_2-PANI/LSA nanocomposites TEM images reveals that the thickness of the PANI shell is quite close in both cases: ~ 6-12 nm and ~ 8-12 nm respectively.

The SEM images (Fig. 2d-e) demonstrate more apparent tendency to form big agglomerates with the size of ~100 – 1000 nm for the DBSA-doped samples than in the case of the LSA dopant (~ 50 – 600 nm). Moreover, individual nanofibers with average diameter of ~50 nm and length up to 3 μm are observed on the LSA-doped nanocomposite surface. Such morphology differences suggest more porous surface of the TiO_2-PANI/LSA nanocomposite due to smaller size of the agglomerates and presence of nanofibers, enhancing sensor responses [35]. This suggestion agrees well with the SSA measurements, which show increased surfaces of 214 and 212.9 m^2/g with the increment of 4 and 2.9 m^2/g for the LSA and DBSA doped nanocomposites respectively as compared with the pristine TiO_2 nanoparticles (210 m^2/g). The difference in the surfaces confirms more porosity of the TiO_2-PANI/LSA nanocomposite.

The nanocomposites structure

The XRD patterns of the pure PANI/DBSA and PANI/LSA (Fig. 3a) contain shoulders at about 18°and two sets of sharp peaks at 2θ = 19.2° / 24.6° and 20.4° / 25° respectively, indicating the partial crystallinity of these polymers [40, 41]. The existing difference in positions and peaks intensities can be explained by the difference in pure PANI structure due to effect of the DBSA and LSA dopants nature.

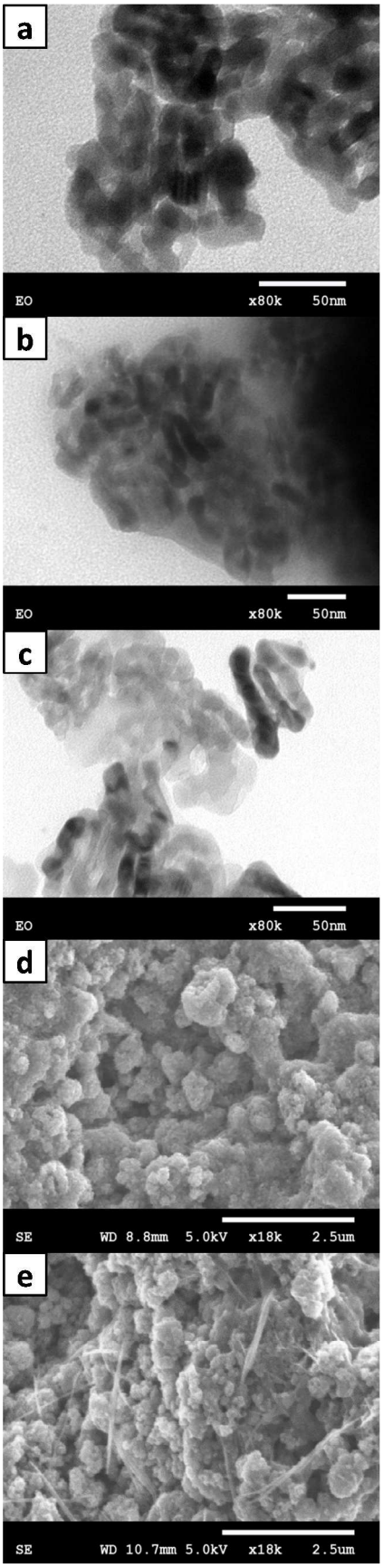

Fig. 2 PANI nanocomposites morphology (**a**) pure TiO_2; (**b,d**) TiO_2-PANI/DBSA; (**c,e**) TiO_2-PANI/LSA.

The nanocomposites XRD patterns demonstrate almost no effect of PANI on the TiO_2 crystallinity (Fig. 3b). At the same time the absence of any PANIs crystalline peaks is observed. The authors of [42] and [43] attribute this phenomenon to aniline adsorption on the surface of nanoparticles leading to molecular chains tethering and thus hampering polyaniline crystallization.

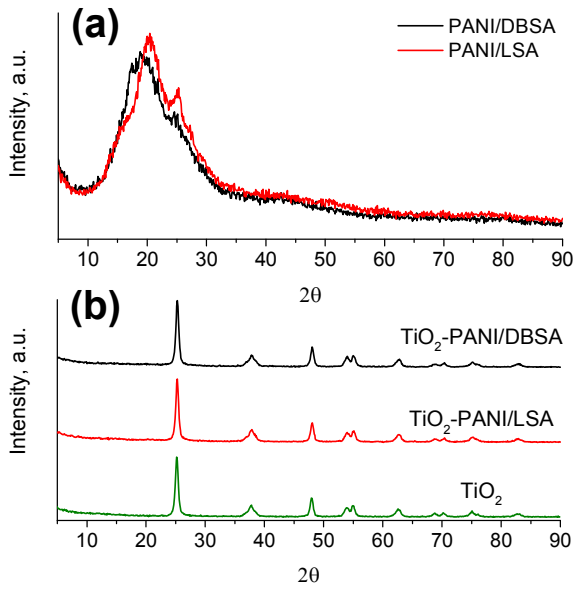

Fig. 3 XRD patterns of (**a**) doped pure polymers; (**b**) TiO_2 powder and PANI nanocomposites

The small-angle X-ray scattering reveals only small differences in structure of the synthesized nanocomposites and pure PANIs (Fig. 4). The similarity of observed intensity decays at $q < 0.14$ A^{-1} suggests the absence of both large-scale and lower-scale structural heterogeneities in PANI nanocomposites [44], whereas the well-resolved SAXS reflections near $q = 0.204$ A^{-1} (PANI/DBSA) and 0.180 A^{-1} (PANI/LSA) corresponding to mean interchain distances of $d = 2\pi/q \approx 3.1$ nm and 3.5 nm respectively can be seen. Summarizing the above, we suggest a specific non-structured polymer condition in the composites due to small thickness of the layers (shells) covering TiO_2 nanoparticles.

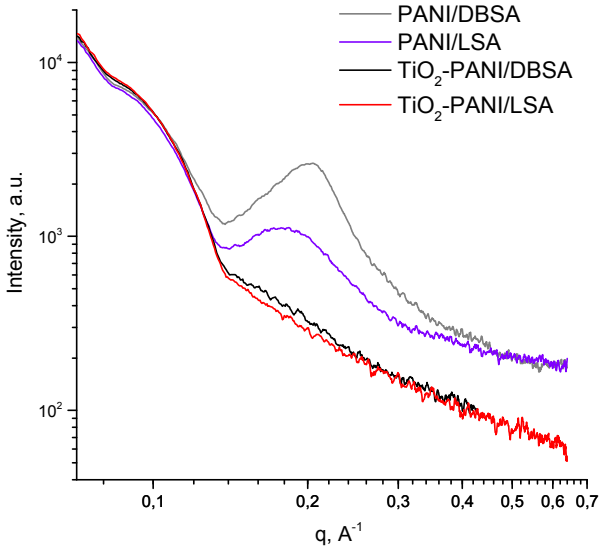

Fig. 4 SAXS patterns of all synthesized materials

FTIR measurements

The FTIR spectra of the both pure PANIs and their nanocomposites contain typical for doped polyaniline bands (Fig. 5). The majority of characteristic peaks demonstrate small red shifts with the change of dopant nature from monoalkyl ester of sulfuric acid (LSA) to aromatic sulfonic acid (DBSA) (Table 1).

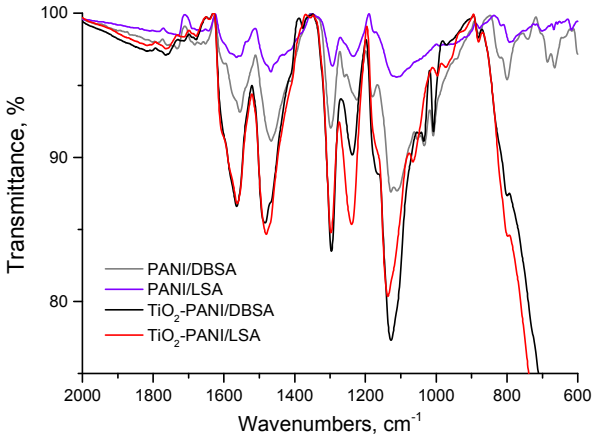

Fig. 5 Survey transmittance FTIR spectra of the synthesized materials

According to Ping [45] such shifts suggest a higher protonation degree of PANI/DBSA. However, some discrepancy observed for C–N stretching vibrations band is most likely due to doping ions size and chemical nature differences.

This suggestion is supported by the fact that positions of C–N ($C–N^{+\cdot}$) stretching vibrations in the presence of TiO_2 nanocrystalline component are considerably less sensitive to the dopant nature (Table 1). Such behaviour can be explained by formation of additional hydrogen bonds between doped polymer and (–OH) groups, inevitably existing on the TiO_2 surface, leading to changes in the peaks shape and the blue-shift of both benzenoid and quinonoid ring bands.

The oxidation degree (OD) estimation, based on quinonoid (D_Q) and benzenoid (D_B) absorption peak heights ratios [46], confirms different electronic states of the PANI backbones in the pure PANIs and their corresponding nanocomposites (Fig. 6).

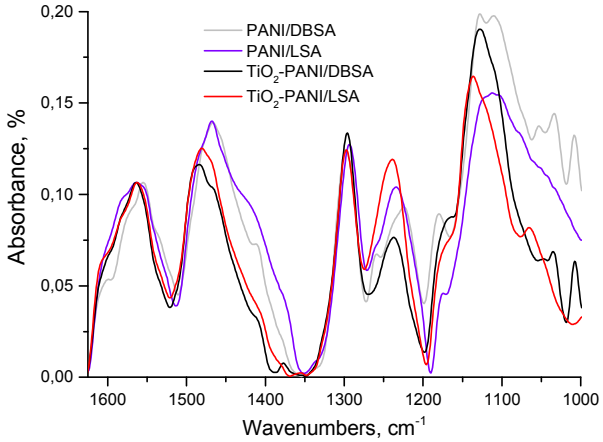

Fig. 6 Normalized absorbance FTIR spectra of the synthesized materials

According to Wei [47], the bands ratio around 80% is typical for emeraldine form and decreases to about 20% for leucoemeraldine. All the materials demonstrate a weak correlation of OD with the dopant nature. However, in case of nanocomposites the OD values are significantly closer to ideal value of 0.5 (Table 2).

Table 2. Oxidation degrees of the pure PANIs and nanocomposites PANI phases

Sample	$OD = D_Q/(D_Q+D_B)$
PANI-DBSA	0.441
PANI-LSA	0.440
TiO_2/PANI-DBSA	0.473
TiO_2/PANI-LSA	0.462

This feature of PANI nanocomposites suggests greater quinodiimine sites quantity in the polymer phase and hence higher protonation degree as compared with pure PANIs. Practically this fact implies stronger nanocomposites responses to the analytes of base nature.

Table 1. The main PANI bands and their assignments [45, 48-51]

PANI/DBSA	PANI/LSA	TiO_2-PANI/DBSA	TiO_2-PANI/LSA	Band assignments
1555	1564	1564	1563	quinonoid ring stretching vibrations (PANI)
1466	1468	1483	1481	benzenoid ring stretching vibrations
1298	1293	1296	1297	C-N stretching vibrations
1224	1234	1237	1239	$C–N^{+\cdot}$ stretching vibrations
1180	1175	shoulder ~1174	shoulder ~1177	C-H in-plane bending vibrations
1029	1115	1130	1136	$Q=N^{+}H–B$ or $B–NH^{+}–B$ vibrations / δ(C–H)
1053	1044 (shoulder)	1048	1166	N=Q=N vibrations, SO_3^-
1034	–	1036	–	S=O stretching
1008	–	1008	–	S=O stretching

*In the low frequency range (< 950 cm^{-1}, not shown here) the small bands of typical PANI C–H vibrations are observed. In case of the nanocomposites these bands are masked by the strong band of Ti-O bending mode of TiO_2 [42]

Sensing properties of the PANI nanocomposites

The sensing behaviour of the synthesized materials was studied at room temperature and different relative humidity (20-80%). All the materials demonstrate reversible responses: their resistance increases under the pollutant exposure and then decreases while the fresh air blowing. The mechanism of these changes is quite well known [52] and in case of ammonia can be schematically expressed by the next equation [53]:

$$PANI\text{-}H^{+}+NH_3 \leftrightarrow PANI+NH_4^{+}$$

In particular, ammonia (or other basic gases e.g. amines) molecules partially withdraw protons from protonated imine groups in the emeraldine salt, thereby changing its electronic properties (conductivity, optical density etc.). In fact, the labile complexes of two bases (ammonia/amines and PANI), protons and charge compensating dopant anions are formed in the sensing clusters of PANI. Naturally, the rate of the interaction between the gas phase and doped PANI depends on the analyte concentration, leading to increase of the sensing material resistance. When the sensing layer is exposed to fresh air again, the complexes decompose into the constituents, the analyte molecules desorb from the sensing material surface and the dopant restores interaction with the PANI chains. This reversible transformation results in restoring of the initial doping degree and resistance of the PANI based sensing material (Fig. 7) [27, 35, 39].

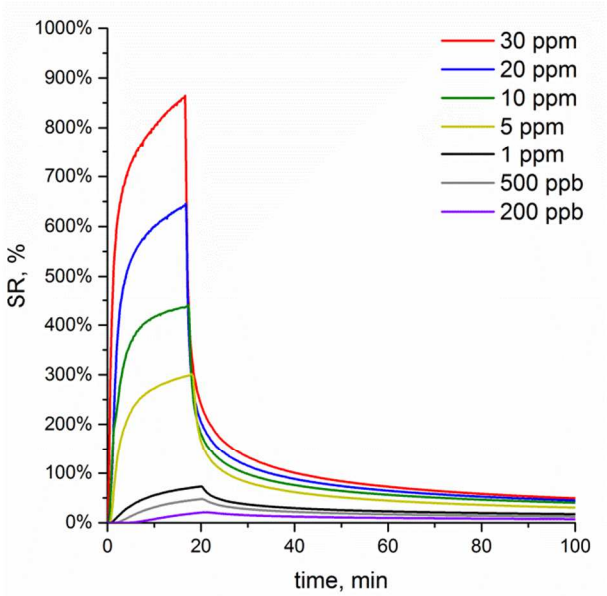

Fig. 7: Typical response of the sensors to ammonia

Fig. 8 compares the responses of the synthesized PANI/DBSA, PANI/LSA and their hybrid nanocomposites with TiO_2. It is clearly seen that the presence of the TiO_2 phase in the nanocomposites leads to a dramatic responses enhancement to ammonia as compared with those of the pure PANIs from ~7.4 times (the PANI/DBSA cases) to ~ 90 times (the PANI/LSA cases). The similar phenomenon was also observed by Tai et al [54, 55] and was attributed to p-n junction formation. The authors postulate that inter-particle interaction causes the reduction of the activation energy and enthalpy of physisorption for ammonia gas leading to the response enhancement. This assumption agrees with our data. However the further investigation of the TiO_2 physical and physicochemical nature effects still needs. Thus, the response enhancements can be also associated with nanocomposites nanostructured nature and porosity.

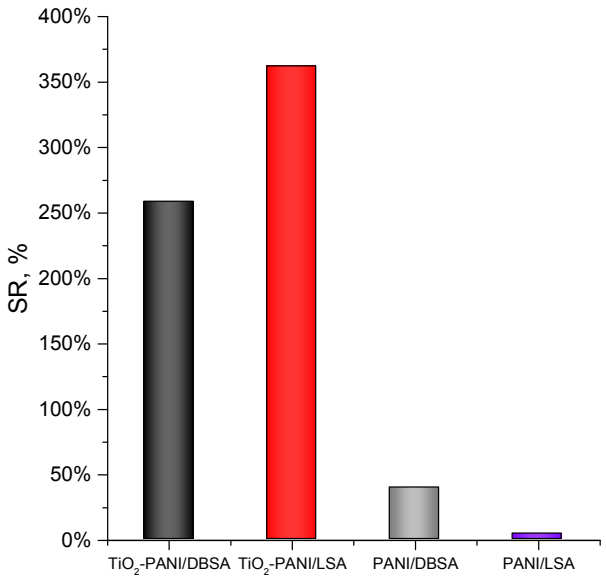

Fig. 8: Response magnitudes comparison of the synthesized materials at 10 ppm of ammonia.

In turn, these additional issues are definitely linked with the dopant chemical nature and size, affecting the synthesized materials responses (Fig.8).

The both nanocomposites show strong responses with good linearity in the tested range (0.2–1ppm), allowing their sensitivity estimation (Fig. 9). This last factor is defined as the slope of the curve representing the sensor response in function of the analyte concentration [56]. The both of synthesized nanocomposites demonstrate responses decrease in the row MA>NH_3>TMA while the basicity of analytes reduces in the row TMA>MA>NH_3. The lowest sensitivity in case of most basic TMA can be explained by interference of molecule dimensions factor. The big size of TMA molecules results in hindered penetration into the dense sensing polymer shell covering the core, especially in case of agglomerated particles occluded by PANI matrix (Fig. 2 d-e).

The observed change in the DBSA and LSA doped samples sensitivity ratio to organic amines and inorganic ammonia probably stems from the specificity of their intermolecular interactions with the different by nature long dodecyl substituent in the benzene ring of “true” sulfonic acid DBSA anions and lauryl (dodecyl) ether group of LSA anions. In the case of the increased sensitivity of the TiO_2/PANI-LSA nanocomposite additional input can be given by its higher SSA as compared with the TiO_2/PANI-DBSA one.

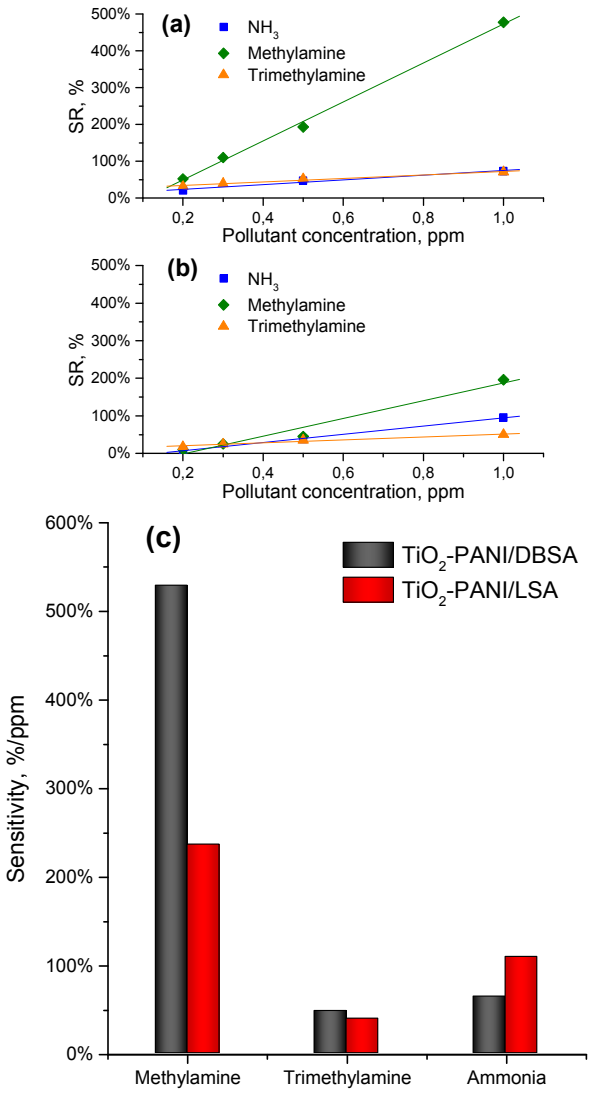

Fig.9: (a) DBSA-doped and **(b)** LSA-doped nanocomposites responses to different pollutants; **(c)** PANI nanocomposites sensitivity comparison

The Fig. 10a shows the sensors responses repeatability to the NH_3 pulses. Despite the observed changes in the baseline signal between ammonia pulses, the resistance returned to its initial value at the end of the experiment. At the same time, it should be emphasized that sensors resistance does not change immediately after the contact with analytes and additionally continues to increase even after the stop of pollutant flow, especially at very low concentrations (Fig. 10b). The observed effect can be explained both by the time lag (~30 s – 4 min) occurred due to the necessity of purging the exposure chamber with a pollutant mixture and by polar nature of ammonia, causing its adsorption on the walls of the system [11-13]. We consider this specificity as the practically important issue of the applied registration conditions. In turn, the latter depends on the geometry of the exposure chamber as well as on the applied protocol of the measurements.

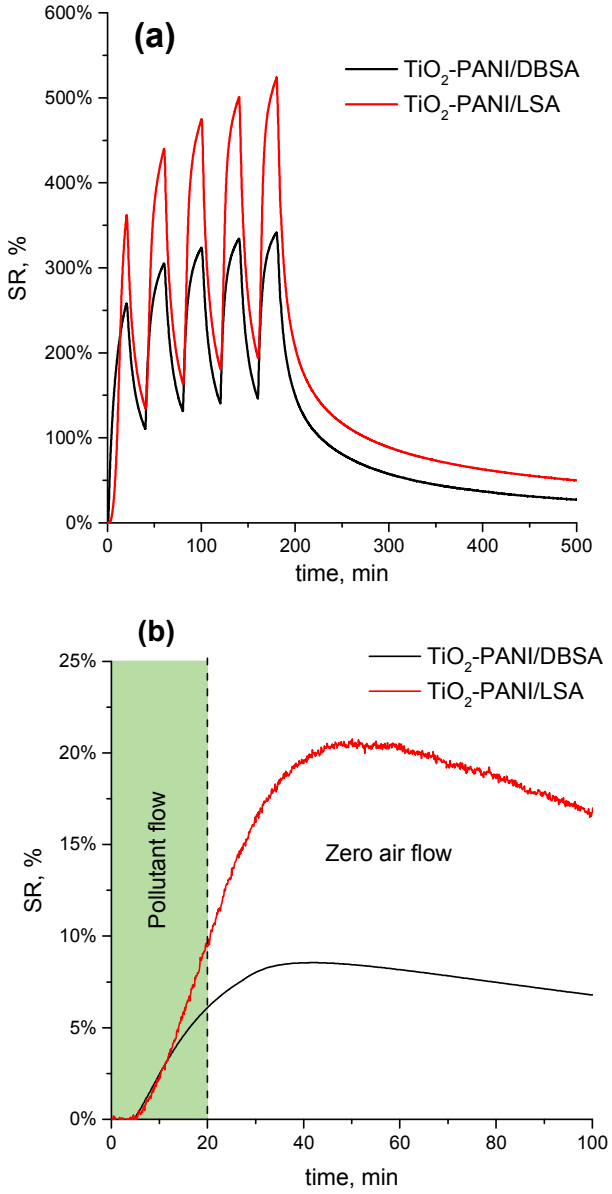

Fig. 10: (a) The nanocomposites response signal repeatability (at 10 ppm of NH_3) and **(b)** signal delay at low ammonia concentrations (20 ppb).

The synthesized materials response dependences on humidity are represented in Fig. 11. The responses of the both pure PANIs grow nonlinearly with the increase of humidity. Such behaviour is usually assigned to PANI physicochemical state and conformation changes, affecting proton hopping and ionic transport along the charged polymer chains [26, 57-59]. It is worth noting that pure PANI/DBSA shows almost one order of magnitude higher response levels comparing to the LSA-doped one (Fig. 11a). Considering weak influence of dopant nature on PANI oxidation degree (Table 2), we suggest that DBSA affects the size of sensitive PANI clusters and thus increasing the total surface more than in PANI/LSA case.

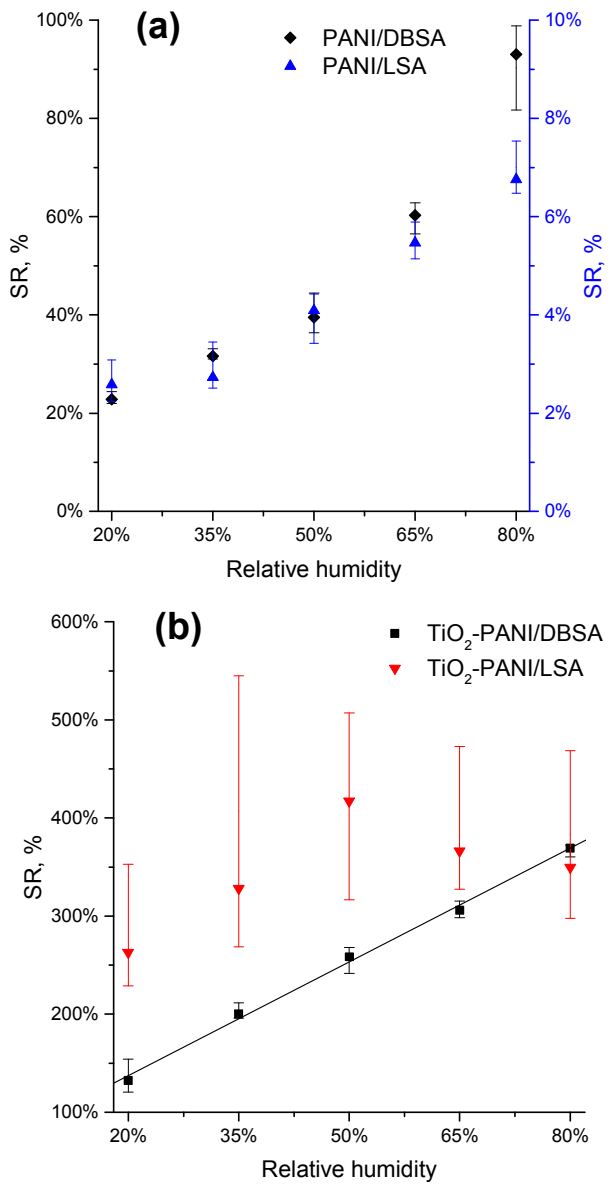

Fig. 11: Response magnitudes comparison of **(a)** pure PANIs and **(b)** PANI based nanocomposites to 10 ppm of ammonia at different humidity.

Along with differences in sensitivity (Figs 8 and 9) the nanocomposites demonstrate distinct from pure PANIs behaviour at various humidity levels (fig. 11b). Thus, the responses to ammonia appear to be rather dependent on the TiO_2 nanoparticles presence than on humidity level and dopant nature. Obviously, the addition of titanium dioxide phase forms highly developed surface facilitating the analyte and moisture contacts with PANI sensing clusters.

The TiO_2-PANI/DBSA nanocomposite has evident linear dependence on humidity (fig. 11b). Probably, it can be attributed to differences in water molecules interaction mechanism with doped PANI at low and high humidity levels, additionally modulated by the TiO_2 surface factor [60]. Though the TiO_2-PANI/LSA nanocomposite shows significantly higher response levels, the large data point's dispersion is observed. During all the 5 cycles of measurements the signal magnitude changed, while the other materials held in the same conditions demonstrate quite good reproducibility. Such signal irreproducibility in case of LSA-doped nanocomposite can be explained by high receptivity of its state to humidity. However, the partial LSA degradation due to use of photocatalitically active TiO_2 anatase nanoparticles is also possible [61-63].

The current quantification limit of 20 ppb for ammonia (fig. 10b) is expected to be improved by further composites optimization. To our knowledge, the analogous systems with PANI nanograins grown on the surface of TiO_2 microfibers demonstrated the lowest detection limit of 50 ppt [36] that testifies to a high practical potentiality of the hybrid PANI nanocomposites with TiO_2. On the other hand, the synthesized in our work hybrid core-shell TiO_2-PANI/dopant nanocomposites are prepared through a convenient inexpensive synthetic technique and can be easily deposited onto electrodes, making them compatible with inexpensive printing technology and roll-to-roll fabrication protocols.

Conclusion

Nanostructured PANI-based composites were prepared via simple chemical aniline polymerization and studied as a sensing layer for electronic polymer based gas sensors operating at room temperature and wide range of humidity. Simple gas sensing array made of interdigitated gold electrodes coated with thin films of nanostructured composites was fabricated. The sensing characteristics were studied at very low ammonia and amines gas concentrations. The synthesized nanocomposites demonstrate high and reversible responses to analytes even at sub-ppm range. The obtained results demonstrate applicability of nanostructured PANI-based nanocomposites with TiO_2 as alternative to conventional sensors for ammonia and amines for applications where ppm and sub ppm concentration detections are needed.

Acknowledgments

Sergei Mikhaylov acknowledges the Mines Douai and University of Lille 1 for PhD scholarship and Armines for the partial financial support.

Alexander Pud, Nikolay Ogurtsov and Yuriy Noskov are grateful to the complex scientific-technical program "Sensing devices for medical–ecological and industrial–technological problems: metrology support and trial operation" of National Academy of Sciences of Ukraine for a partial financial support.

Notes and references

[a] Institute of Bioorganic Chemistry and Petrochemistry, National Academy of Sciences of Ukraine, 50 Kharkovskoe Shosse, 02160, Kiev, Ukraine.
[b] Mines Douai, Département Sciences de l'Atmosphère et Génie de l'Environnement (SAGE), 941 rue Charles Bourseul, F-59508 Douai, France.
* Corresponding authors; E-Mail: jean-luc.wojkiewicz@mines-douai.fr, Tel.: + 03 27 71 23 33; pud@bpci.kiev.ua, Tel.: +38 044 559 70 03; Fax: + 38 044 573 25 52.

See DOI: 10.1039/b000000x/

1. E. Stokstad, *Science*, 2014, **343**, 238.
2. Nino Künzli, Laura Perez and R. Rapp, *Air Quality and Health*, European Respiratory Society, 2010.
3. C. J. Nielsen, H. Herrmann and C. Weller, *Chemical Society Reviews*, 2012, **41**, 6684-6704.
4. D. Lee and A. S. Wexler, *Atmospheric Environment*, 2013, **71**, 95-103.

5. C. Qiu and R. Zhang, *Physical Chemistry Chemical Physics*, 2013, **15**, 5738-5752.
6. X. Tang, D. Price, E. Praske, S. A. Lee, M. A. Shattuck, K. Purvis-Roberts, P. J. Silva, A. Asa-Awuku and D. R. Cocker Iii, *Atmospheric Environment*, 2013, **72**, 105-112.
7. H. Hellén, A. J. Kieloaho and H. Hakola, *Atmospheric Environment*, 2014, **94**, 192-197.
8. G. Chen, J. Liu, M. Liu, G. Li, Z. Sun, S. Zhang, C. Song, H. Wang, Y. Suo and J. You, *Journal of Chromatography A*, 2014, **1352**, 8-19.
9. E. Jazan and H. Mirzaei, *Journal of Pharmaceutical and Biomedical Analysis*, 2014, **88**, 315-320.
10. M. Mäkinen, M. Sillanpää, A. K. Viitanen, A. Knap, J. M. Mäkelä and J. Puton, *Talanta*, 2011, **84**, 116-121.
11. J. Wang, W. Zhang, L. Li and Q. Yu, *Appl. Phys. B*, 2011, **103**, 263-269.
12. M. B. Pushkarsky, M. E. Webber, O. Baghdassarian, L. R. Narasimhan and C. K. N. Patel, *Appl. Phys. B*, 2002, **75**, 391-396.
13. T. Hibbard and A. J. Killard, *Journal of Breath Research*, 2011, **5**, 037101.
14. C. Popa, D. C. A. Dutu, R. Cernat, C. Matei, A. M. Bratu, S. Banita and D. C. Dumitras, *Appl. Phys. B*, 2011, **105**, 669-674.
15. C. Jiang, R. Liu, G. Han and Z. Zhang, *Chemical Communications*, 2013, **49**, 6647-6649.
16. Y. Han, S. Liu, B. Liu, C. Jiang and Z. Zhang, *RSC Advances*, 2014, **4**, 2776-2782.
17. S. Liu, C. Jiang, B. Yang, Z. Zhang and M. Han, *RSC Advances*, 2014, **4**, 42358-42363.
18. L. Zhang, C. Jiang and Z. Zhang, *Nanoscale*, 2013, **5**, 3773-3779.
19. S.-A. Leung and A. J. de Mello, *Journal of Chromatography A*, 2002, **979**, 171-178.
20. A. R. Fakhari, M. C. Breadmore, M. Macka and P. R. Haddad, *Analytica Chimica Acta*, 2006, **580**, 188-193.
21. A.-A. Peláez-Cid, S. Blasco-Sancho and F.-M. Matysik, *Talanta*, 2008, **75**, 1362-1368.
22. Pawar S. G., Chougule M. A., Patil S. L., Raut B. T., Godse P. R., Sen S. and Patil V. B., *Sensors Journal, IEEE*, 2011, **11**, 3417-3423.
23. Pawar S. G., Patil S. L., Chougule M. A., Raut B. T., Godase P. R., Mulik R. N., Sen S. and Patil V. B., *Sensors Journal, IEEE*, 2011, **11**, 2980-2985.
24. E. M. K. Arshak, G.M. Lyons, J. Harris, S. Clifford, *Sensor Review*, 2004, **24**, 181-198.
25. Hua Bai and G. Shi, *Sensors*, 2007, **7**, 267-307.
26. G. Rizzo, A. Arena, N. Donato, M. Latino, G. Saitta, A. Bonavita and G. Neri, *Thin Solid Films*, 2010, **518**, 7133-7137.
27. M. Joubert, M. Bouhadid, D. Bégué, P. Iratçabal, N. Redon, J. Desbrières and S. Reynaud, *Polymer*, 2010, **51**, 1716-1722.
28. G. D. Khuspe, D. K. Bandgar, S. Sen and V. B. Patil, *Synthetic Metals*, 2012, **162**, 1822-1827.
29. P. P. Sengupta, P. Kar and B. Adhikari, *Thin Solid Films*, 2009, **517**, 3770-3775.
30. K. Chatterjee, P. Dhara, S. Ganguly, K. Kargupta and D. Banerjee, *Sensors and Actuators B: Chemical*, 2013, **181**, 544-550.
31. I. Izzuddin, N. Ramli, M. M. Salleh, M. Yahaya and M. H. Jumali, Semiconductor Electronics, 2008. ICSE 2008. IEEE International Conference on, 2008.
32. G. D. Khuspe, S. T. Navale, M. A. Chougule and V. B. Patil, *Synthetic Metals*, 2013, **185–186**, 1-8.
33. V. Talwar, O. Singh and R. C. Singh, *Sensors and Actuators B: Chemical*, 2014, **191**, 276-282.
34. S. L. Patil, M. A. Chougule, S. Sen and V. B. Patil, *Measurement*, 2012, **45**, 243-249.
35. J. L. Wojkiewicz, V. N. Bliznyuk, S. Carquigny, N. Elkamchi, N. Redon, T. Lasri, A. A. Pud and S. Reynaud, *Sensors and Actuators B: Chemical*, 2011, **160**, 1394-1403.
36. Gong Jian, Li Yinhua, Hu Zeshan, Zhou Zhengzhi and D. Yulin, *The Journal of Physical Chemistry C*, 2010, **114**, 9970-9974.
37. A. Pud, N. Ogurtsov, A. Korzhenko and G. Shapoval, *Progress in Polymer Science*, 2003, **28**, 1701-1753.
38. P. P. Sengupta and B. Adhikari, *Materials Science and Engineering: A*, 2007, **459**, 278-285.
39. T. Mérian, N. Redon, Z. Zujovic, D. Stanisavljev, J. L. Wojkiewicz and M. Gizdavic-Nikolaidis, *Sensors and Actuators B: Chemical*, 2014, **203**, 626-634.
40. Pouget J. P., Jozefowicz M. E., Epstein A. J., Tang X. and MacDiarmid A. G., *Macromolecules*, 1991, **24**, 779-789.
41. N. A. Ogurtsov, Y. V. Noskov, K. Y. Fatyeyeva, V. G. Ilyin, G. V. Dudarenko and A. A. Pud, *The Journal of Physical Chemistry B*, 2013, **117**, 5306-5314.
42. H. Xia and Q. Wang, *Chemistry of Materials*, 2002, **14**, 2158-2165.
43. S. Nasirian and H. Milani Moghaddam, *Polymer*, 2014, **55**, 1866-1874.
44. V. P. Privalko, S. M. Ponomarenko, E. G. Privalko, S. V. Lobkov, N. A. Rekhteta, A. A. Pud, A. S. Bandurenko and G. S. Shapoval, *Journal of Macromolecular Science, Part B*, 2005, **44**, 749-759.
45. Z. Ping, *Journal of the Chemical Society, Faraday Transactions*, 1996, **92**, 3063-3067.
46. Epstein A. J., McCall R. P., Ginder J. M. and MacDiarmid A. G., *Spectroscopy and Photoexcitation Spectroscopies of Polyaniline: A Model System for New Phenomena*, Defense Technical Information Center, Ft. Belvoir, 1991.
47. Y. Wei, K. F. Hsueh and G. W. Jang, *Macromolecules*, 1994, **27**, 518-525.
48. M. Trchová and J. Stejskal, *Pure and Applied Chemistry*, 2011, **83**, 1803-1817.
49. M. Trchová, Z. Morávková, I. Šeděnková and J. Stejskal, *Chem. Pap.*, 2012, **66**, 415-445.
50. K. G. Neoh, M. Y. Pun, E. T. Kang and K. L. Tan, *Synthetic Metals*, 1995, **73**, 209-215.
51. Y.-C. Lin, F.-H. Hsu and T.-M. Wu, *Synthetic Metals*, 2013, **184**, 29-34.
52. D. Nicolas-Debarnot and F. Poncin-Epaillard, *Analytica Chimica Acta*, 2003, **475**, 1-15.
53. H. Kebiche, D. Debarnot, A. Merzouki, F. Poncin-Epaillard and N. Haddaoui, *Analytica Chimica Acta*, 2012, **737**, 64-71.
54. H. Tai, Y. Jiang, G. Xie, J. Yu and X. Chen, *Sensors and Actuators B: Chemical*, 2007, **125**, 644-650.
55. H. Tai, Y. Jiang, G. Xie, J. Yu, X. Chen and Z. Ying, *Sensors and Actuators B: Chemical*, 2008, **129**, 319-326.
56. F.-G. Banica, *Chemical Sensors and Biosensors: Fundamentals and Applications*, John Wiley & Sons, 2012.
57. S. Jain, S. Chakane, A. B. Samui, V. N. Krishnamurthy and S. V. Bhoraskar, *Sensors and Actuators B: Chemical*, 2003, **96**, 124-129.
58. E. Danesh, F. Molina-Lopez, M. Camara, A. Bontempi, A. V. Quintero, D. Teyssieux, L. Thiery, D. Briand, N. F. de Rooij and K. C. Persaud, *Analytical Chemistry*, 2014, **86**, 8951-8958.
59. F.-W. Zeng, X.-X. Liu, D. Diamond and K. T. Lau, *Sensors and Actuators B: Chemical*, 2010, **143**, 530-534.
60. N. Parvatikar, S. Jain, S. Khasim, M. Revansiddappa, S. V. Bhoraskar and M. V. N. A. Prasad, *Sensors and Actuators B: Chemical*, 2006, **114**, 599-603.
61. X. Li, D. Wang, G. Cheng, Q. Luo, J. An and Y. Wang, *Applied Catalysis B: Environmental*, 2008, **81**, 267-273.
62. M. Radoičić, Z. Šaponjić, I. A. Janković, G. Ćirić-Marjanović, S. P. Ahrenkiel and M. I. Čomor, *Applied Catalysis B: Environmental*, 2013, **136–137**, 133-139.
63. Y. Lin, D. Li, J. Hu, G. Xiao, J. Wang, W. Li and X. Fu, *The Journal of Physical Chemistry C*, 2012, **116**, 5764-5772.

